Journal of Agriculture and Food Research 24 (2025) 102497

Contents lists available at ScienceDirect

Journal of Agriculture and Food Research

journal homepage: www.sciencedirect.com/journal/journal-of-agriculture-and-food-research

A new approach in monitoring regional water use efficiency in response to climate variability: a case study in Hungary

Angura Louis [a,b,*], Zsolt Zoltán Fehér [a,b], Tamás János [a,b], Attila Nagy [a,b]

[a] Institute of Water and Environmental Management, Faculty of Agricultural and Food Sciences and Environmental Management, University of Debrecen, Böszörményi str. 138., H-4032, Debrecen, Hungary

[b] National Laboratory for Water Science and Water Safety, Institute of Water and Environmental Management, Faculty of Agricultural and Food Sciences and Environmental Management, University of Debrecen, Böszörményi str. 138., H-4032, Debrecen, Hungary

ARTICLE INFO

Keywords:
Regional hydrology
WUE
Biomass soil moisture index
Climate variability

ABSTRACT

This study develops and evaluates a biomass soil moisture index (NWUESM) for determining water use efficiency (WUE) that is less expensive and simplier to compute than the standard regional WUE indicator (RWUEEC). The research uses a section of the Tisza-Körös valley irrigation system region (TIKEVIR) in northeastern Hungary as a case study site. NWUESM is computed as a ratio of Normalized Difference Vegetation Index (NDVI) to volumetric soil moisture content at 30 cm and 60 cm soil depths respectively and actual regional WUE (RWUEEC) as a ratio of Gross primary productivity (GPP) to actual evapotranspiration (ET). NWUESM (30 cm) and NWUESM (60 cm) showed consistent positive correlation and alignment with RWUEEC trends over time with however NWUESM (60 cm) demonstrating superior accuracy compared to NWUESM (30 cm) as a proxy for computing and predicting RWUEEC. Correlation between RWUEEC and predicted regional WUE (RWUEEC Pred) at 60 cm yielded higher R^2 values of 0.9956 for 2018, 0.9486 for 2020, and 0.9452 for 2022 with lower RMSE of 0.038 for 2018, 0.0686 for 2020, and 0.0576 for 2022. In contrast, the correlation between RWUEEC Pred at 30 cm and RWUEEC yielded R^2 values of 0.9817 for 2018, 0.9333 for 2020, and 0.761 for 2022, with RMSE values of 0.0777 for 2018, 0.0782 for 2020, and 0.2529 for 2022 respectively. Water productivity peaked around June and July in the test area reflecting optimal growing conditions for crops and thus water through irrigation should reach 60 cm depth due to soil moisture stability.

1. Introduction

Monitoring regional water use efficiency is essential to managing water scarcity challenges for food production in the face of climate change by optimizing water use at farm and landscape levels. Water scarcity and climate variability are becoming major challenges, impacting farming, and posing serious threats to food security according to FAO [1]. The global agricultural sector ranks the highest water intensive utilizer with 70 % of the freshwater withdrawals in meeting the global food demands according to FAO [2]. The increased uncertainties in agricultural crop production accelerated by climate change and variability; shifts rainfall patterns, increasing temperatures, and extreme weather events such as droughts, that exacerbate more stress on the limited water resources in crop production. This impacts the livelihoods of rural communities, and the stability of economies and the overall health of the ecosystem [3]. According to the United Nations (UN) water report of 2021 [4], more than 2 billion people derive their livelihoods from agriculture and about 4 billion people lack water for at least one month each year. This water crisis and scarcity are evident in water stressed regions like sub-Saharan Africa and south Asia where rain-fed agriculture is the major practice. The world bank in 2022 [5] reported a 50 % reduction in agricultural productivity of staple cereal crops such as corn and sorghum due to the impacts of drought in sub-Saharan Africa. In some other regions like south Asia, declining groundwater levels have been noticed and the occurrence of erratic monsoons, reducing wheat and rice yields. These yields have been projected to have a percentage drop of about 15–20 % by 2050 in case severe climate change impacts continue taking place [6]. The European environment agency (EEA) in 2022, also reported Europe to be experiencing water scarcity in its agricultural sector where countries like

* Corresponding author. Institute of Water and Environmental Management, Faculty of Agricultural and Food Sciences and Environmental Management, University of Debrecen, Böszörményi str. 138., H-4032, Debrecen, Hungary.

E-mail address: angura.louis@agr.unideb.hu (A. Louis).

https://doi.org/10.1016/j.jafr.2025.102497
Received 17 April 2025; Received in revised form 22 October 2025; Accepted 30 October 2025
Available online 31 October 2025

Hungary in the Carpathian basin have recorded a six-fold increment in drought affected areas since 2000 [7]. Within Hungary, the TIKEVIR region, located in the Great Hungarian Plain, show cases one of the most vulnerable agricultural zones in central Europe due to the nature of its flat terrain with low natural water retention abilities, and high reliance on surface and groundwater irrigation. Previous years have seen enormous yield variability and decline in major irrigation dependent crops like maize, sunflower, and wheat, largely caused by reduced precipitation, prolonged summer droughts, and over-extraction of water from the rivers Danube and Tisza respectively, both of which have shown declining water levels [7]. These regional examples of climate variability show the larger trend of climate-driven agricultural stress and underscore the pressing need for resilient farming methods and adaptive water management in the TIKEVIR case study region.

Addressing these issues in the TIKEVIR crop production landscape requires a focus on enhancing water use efficiency (WUE), to effectively utilize the limited water resources in producing more food for the people [8]. Elfarkh et al. [9] highlighted the importance of monitoring WUE in seeking to optimize irrigation, due to its representation of water loss into the atmosphere from crop canopies relative to the biomass produced. Agricultural water productivity enhancement requires critical understanding of WUE's across different scales such as crop growth (physiological), yield (biomass), soil-plant-water interactions (ecosystem) and regional landscapes [10]. Among these indicators, WUE in different agroecosystems across various scales can be computed as ratios of production to water variables [10]. At the physiological scale focusing on plant-level processes, WUE is represented by net photosynthesis (carbon gain) to transpiration ratio [11]**.** The biomass scale represents WUE as ratios of forage production to precipitation, grain yield to irrigation, and above ground biomass to evapotranspiration, all aimed at assessing water inputs relative to crop growth and yield [12]. At the ecosystem scale, broader productivity measurement ratios are used such as net ecosystem production to precipitation ratio and Gross primary production to evapotranspiration ratio to reflect water use at the level of the entire ecosystems [13]. On larger landscapes, remote sensing indices and weather variables such as Normalized Difference Vegetation Index (NDVI) to gridded precipitation ratio and NDVI to modeled evapotranspiration (ET) ratio are used to gauge productivity over extensive areas [14,15]. Lastly is the supply chain scale which expresses WUE as a ratio of water productivity to water footprint aimed at capturing the water required across all stages of production relative to output [10]. These ratios provide useful indication for water resource management across different scales, for optimization and sustainable agricultural practices.

Never the less, each of these WUE approaches has inherent methodological advantages and limitations that affect their practical application. Physiological and biomass scale WUE measurement methods, offer accurate estimates of WUE's, but are highly localized and dependent on destructive sampling of vegetation tissues and require controlled environmental measurements, making them unsuitable for large-scale monitoring [12]. On the other hand, ecosystem and regional scale WUE measurement approaches based on eddy covariance and modeled ET offer broader spatial insight but require costly instrumentation and are sensitive to parameter uncertainties, particularly under heterogeneous landscapes [16,17]. Further, remote sensing-based indices, such as NDVI/ET, provide extensive coverage and temporal continuity but may overestimate productivity under stressed vegetation conditions, and as such could result into misrepresentation of water use in areas with limited ET data [14]. These limitations create a methodological gap between high accuracy local measurements and spatially continuous, cost-effective, and scalable WUE monitoring.

Many studies have pinpointed the necessity of remote sensing in mitigating the climate change crisis through the integration of satellite imagery and other advanced water management strategies [18,19]. The commonly used regional WUE indicator measured as Gross primary productivity (GPP) to evapotranspiration (ET) ratio gives a crucial understanding of ecosystem WUE but is limited under changing climates and diverse environmental conditions [20]. For example, during dry and drought periods, the GPP to ET ratio inadequately captures the true WUE of an ecosystem [17,20]. It is also an expensive method for estimating WUE due to the high costs of sophisticated equipment like infrared gas analyzers, lysimeters, energy flux sensors and complex data processing with the requirement of skilled labor and site-specific calibration [16]. A cheaper and easier to compute method is needed to help farmers and policy makers in monitoring WUE's to enhance crop water productivity in their farming systems. One of these possibilities in irrigated agriculture is that decisions pertaining to crop water supplementation could be based on the assessments of soil moisture content to directly link the soil water availability to crop water needs over space and time [21] and monitor how effectively vegetation converts water into biomass and yield across different cycles of crop growth. According to Magyar et al. [22] highlighted that soil moisture dynamics and water fluxes greatly affect crop production which needs careful management in irrigated agriculture. This could be vital in providing valuable insights into the interactions between ecosystems, water resources, and agricultural productivity on a regional scale. Despite the paramount importance, there is still a gap in understanding the spatial and temporal variability of WUE under changing climatic conditions [20] where traditional methods based on ground measurements, are limited by their spatial coverage and are labor-intensive [23,24]. This creates a need for more efficient, scalable methods to monitor water use accurately and consistently across larger areas and over extended time periods [25].

By monitoring the volumetric soil moisture content, critical real-time data on the water status measured in the root zone can be provided to help in optimizing irrigation, and ensure crops receive sufficient water for growth and yield while minimizing water wastage from over-irrigation and runoff [26]. This precision, however, needs to be evaluated over space and time in evaluating how effectively vegetation converts water into biomass and yield. Remote sensing could present valuable opportunities to fill these gaps, offering tools to measure vegetation and soil moisture levels over vast regions and timeframes [27]. By integrating remotely sensed data with ground information, it could be possible to estimate and forecast WUE's at regional scales and provide critical data to optimize water resource management and agricultural practices in the face of climate variability [28].

In response to these methodological deficiencies, this research develops and introduces the biomass soil moisture index (NWUESM), computed as a ratio of NDVI to volumetric soil moisture (SM) and illustrate how WUE fluctuates with seasonal changes and varying moisture conditions during cropping periods. The NWUESM approach allows for the dynamic evaluation of vegetation-water interactions under varying climatic situations by combining the spatial continuity of vegetation indicators with the physical relevance of soil water availability. Unlike GPP/ET and other modeled indices approaches, NWUESM utilizes readily available satellite and ground-based soil moisture data, making it computationally simple, low-cost, and scalable. This novel indicator directly reflects vegetation response to actual soil water status, providing a more sensitive representation of ecosystem WUE during dry spells, irrigation events, and crop growth cycles. Therefore, NWUESM serves as an innovative and empirical approach to bridge the gap between physiological realism and spatial monitoring for agricultural water management. This indicator tool could be integrated into remote sensing time series at the watershed level to enhance agricultural sustainability, improve water management, and help monitor seasonal water use in crop production. This will help to better understand changes in water demand, ensure effective irrigation, optimize water resources, and increase crop yield.

2. Materials and methods

2.1. Study area

In this study, a section of the Tisza-Körös valley irrigation system region (TIKEVIR) measuring 4111.59 km^2 was considered due to the intensity of agricultural activities carried out in this area. The test site is a very crucial irrigation zone in the northeastern Great Hungarian Plain, for supporting agriculture and water resources management in Hungary [29]. The region experiences a temperate continental climatic condition with four different seasons of spring, summer, autumn and winter, and receives an annual precipitation of between 500 and 700 mm and solar radiation of between 1200 and 1600 h respectively [30]. The amount of precipitation and other meteorological variables vary per season; during spring, temperatures range between 4 °C and 20 °C, with rainfall of 30–50 mm per month and volumetric soil moisture content of 26.3 V/V % at 30 cm depth and 24.5 V/V % at 60 cm depth. Temperatures in the summer range between 20 °C and 35 °C, with relative humidity of between 60 and 70 %, volumetric soil moisture content of 20.3 V/V % at 30 cm depth and 22.1 V/V % at 60 cm depth and wind speed of 2–4 m/s. Autumn season cools from 20 °C to 5 °C, with rainfall ranging between 30 and 40 mm per month, relative humidity of 60–65 % and volumetric soil moisture content of 20.1 V/V % at 30 cm depth and 21.1 V/V % at 60 cm depth respectively. The winter season is the coldest season with occasional snowfall and temperatures ranging between −2 °C and −5 °C, with relative humidity of 80–90 %, and volumetric soil moisture content of 30.3 V/V % at 30 cm depth and 27.5 V/V % at 60 cm depth [30].

This region is characterized by a network of water canals, reservoirs, and flood control water pumping stations that utilize water from the rivers Tisza, Keleti and Körös respectively and accounts for about 25 % of the food produced in Hungary according to the Hungarian central statistical office [31], making it a vital assert for both national food security and economic sustainability [32]. The common crops grown in this region are but not limited to maize, wheat, sunflower, and vegetables with over 2000 km^2 of arable land under irrigation [31,33]. Despite its vitality, the region faces several challenges, especially climate change impacts that trigger frequent droughts, rainfall unpredictability, and in some cases, in-land excess water is experienced [34]. These impacts strain the irrigation infrastructure's capacity to provide a stable water supply for irrigation while protecting agricultural production from water-related disasters. In addition, the region experiences inefficient water use due to outdated irrigation techniques employed that lead to water wastage [35]. Since then, programs like Széchenyi 2020 have been initialized by the Hungarian government to support water management related projects aimed at improving the infrastructure and water resources efficiency in the country. These issues must be tackled to support the agricultural productivity and environmental resilience of the TIKEVIR region to secure food security and the economy of Hungary.

2.2. Crops and growth cycles in the test site

Evaluating water use efficiency in the test site required detailed knowledge of the crop production cycles and root zone depths for the crops (Tables 1 and 2). The major crops grown in this region include but are not limited to corn, sunflowers, winter wheat, woody and fruit trees, and grasslands [31]. Maize (Corn), normally planted in April, has a growing season extending from April to September and harvested between late September and October [1]. Sunflowers are sown from the middle of April to early May and grow up to late August and September to harvest. Winter wheat, planted between September and October, grows from March to July and is harvested between late June to July [1]. Wood and fruit trees are perennial, with their growth spanning from April to September, and then harvested between late September and October [1]. Annual and perennial grasslands have two main sowing periods (March to April and August to September) and are maintained from March to November, enabling multiple harvests and cuts between May and October (Table 1). Understanding these production cycles within the region is vital for assessing the timing of peak water demands, crop growth stages, and harvest periods, which directly influences crop water productivity.

Table 1
Crop production calendar for the dominant agricultural categories in the test site.

S/No	Crop Type	Sowing Time	Growing Season	Days	Harvest period
1	Corn	Apr	Apr–Sept	150–180	Late Sept–Oct
2	Sunflower	Mid Apr - Early May	Apr–Aug/Sept	130–150	Late Aug–Sept
3	Winter wheat	Sept–Oct	Mar–Jul	230–280 inclusive of overwintering period	Late Jun–Jul
4	Trees	Perennial	Apr–Sept	170 -240 only active growth period	Late Sept–Oct
5	Grasslands	Perennial (For new sowing Mar–Apr, Aug–Sept)	Mar/Apr–Oct/Nov	200–240	May–Oct

Table 2
The rootzone depth consideration for the dominant agricultural categories in the test site.

S/No	Crop Type	Root zone depth (cm)	Soil moisture monitoring depth (cm)
1	Corn	60–120	30, 60
2	Sunflower	90–180	30, 60
3	Winter wheat	30–120	30, 60
4	Trees	60–120+	30, 60
5	Grasslands	30–60	30, 60

The water extractions from the soil by these crop categories are also heavily impacted by the levels of their root depths, thus it's important to give special consideration to the crop root zone depth in monitoring soil moisture for optimized irrigation (Table 2). The varying root depths of each crop category influences their water uptake, for example corn has a root depth of between 60 and 120 cm, while sunflowers and trees have deeper root zones ranging from 90 to 180 cm and 60 to more than 150 cm, respectively [36,37]. Winter wheat and grasslands have shallower root zones, ranging from 30 to 120 cm and 30–60 cm, respectively [38]. Therefore, to cater for the entire regional ecosystem WUE, soil moisture monitoring was conducted at depths of 30 and 60 cm for all crops to capture the critical zones where roots absorb water (Table 2). These measurements were crucial in evaluating soil moisture levels during different growth stages for all the five cropping periods from 2018 to 2022.

In our study, we monitored and modeled soil moisture at 30 cm and 60 cm respectively to represent the upper and mid-root zones where most plant water uptake occurs in field conditions. Some research studies in the Carpathian Basin showed that over 75 % of crop evapotranspiration originated within the top 60 cm of soil [21,39], regardless of the deep-rooted species [40]. The 30 cm root depth captures rapid surface moisture changes influencing NDVI, while 60 cm root depth reflects the sustained moisture supporting growth. For deep-rooted crops like sunflower and trees, this may underrepresent deeper water use greater than 90 cm, but NWUESM primarily targets the soil depths driving canopy-level vegetation response observable via remote sensing.

A thorough validation of the index under uniform measurement settings was made possible by standardizing soil-moisture depths to 30 cm and 60 cm. This also guaranteed consistent data comparability across crop varieties, seasons, and sensor recordings.

2.3. Research workflow

The workflow adopted in this study uses ground-based and remotely sensed data as shown in Fig. 2. The process begins with the acquisition of reference volumetric soil moisture content (SM) and meteorological data such as rainfall from a network of six meteorological stations run by the Hungarian drought monitoring services (HU drought monitoring system) and KITE, an agricultural service provider (Fig. 1b). Meteorological Stations 1 to 5 (Fig. 1b) are operated by the Hungarian drought monitoring system, which provides open access to hourly meteorological data. In contrast, Station 6 (Fig. 1b) is managed by KITE that provides data upon request, with measurements collected at 10-min intervals. The second type of data is sourced from Moderate Resolution Imaging Spectroradiometer (MODIS) satellite, providing estimates of NDVI, ET and GPP (Fig. 2). The higher temporal resolution and global coverage of MODIS - NDVI allowed for detailed monitoring of vegetation dynamics and ecosystem changes, while MODIS - GPP provided valuable insights into ecosystem productivity and carbon fluxes, essential for assessing climatic and ecological variables.

Ratios of these variables are then computed as RWUEEC (GPP/ET), NWUESM (NDVI/SM at 30 cm and 60 cm respectively) and used as data input into a Fourier series regression model, where time variables and Fourier terms are generated to capture seasonal trends of WUE (Fig. 2). RWUEEC is the actual regional WUE used as a benchmark WUE indicator whereas NWUESM is the newly developed biomass soil moisture indicator for calculating WUE. The performance of the model is then evaluated using error metrics such as coefficient of determination (R^2), mean squared error (MSE), mean absolute error (MAE), root mean squared error (RMSE), and normalized root mean square error (NRMSE). Finally, the predicted values of RWUEEC using input data of NWUESM at 30 cm and 60 cm respectively are compared with actual observations of benchmark indicator (RWUEEC) to assess the model's accuracy and reliability (Fig. 2). In this study, rainfall data was also considered in assessing NDVI and soil moisture content, as it directly influences soil water availability and vegetation growth.

2.4. Data acquisition

2.4.1. Soil moisture

The volumetric soil moisture content was downloaded from the drought monitoring system of Hungary and KITE data archives. These meteorological stations use soil moisture sensors with probes placed at various depths to measure moisture levels. The sensors work by detecting the dielectric constant of soil, which changes based on the water content, using Time-Domain Reflectometry (TDR) method to measure the speed of electrical signals through the soil [41]. Data is acquired regularly at 1 h's intervals for the Hungarian drought monitoring system and 10-min interval for the KITE meteorological station, providing high temporal resolution for real-time soil moisture monitoring.

2.4.2. NDVI data

Time series data on the NDVI for the years 2018, 2019, 2020, 2021 and 2022 were sourced from the MODIS product (MODIS/MCD43A4_006_NDVI) in accordance with Eq. (1) at a spatial resolution of 500m whose daily vegetation observation is provided as a 16-day temporal composites [42]. All this data was obtained using google earth engine application programming interface by applying filters to extract the relevant NDVI values and ensuring temporal consistency, while considering only cloud free images throughout the cropping periods from march to October in each reference year of 2018–2022. The extraction of these values was in accordance to Kriegler et al. [43].

$$\mathrm{NDVI} = \frac{(\mathrm{NIR} - \mathrm{RED})}{(\mathrm{NIR} + \mathrm{RED})} \tag{1}$$

where NDVI is the Normalized Difference Vegetation Index, NIR is the reflectance value from the near-infrared band (Band 2) and Red is the reflectance value from the red band (Band 1) of the electromagnetic spectrum.

The overall goal for NDVI estimation was to provide insights into crop health, growth patterns, and the ecosystem conditions, enabling data-driven decisions to be made in agricultural production. This aims at improving irrigation management by allowing precise monitoring of crop water needs throughout the cropping periods. By this analysis, the vegetation vigor and identification of areas with low NDVI, water stressed areas were identified as a strategy to enhance resilience to climate change.

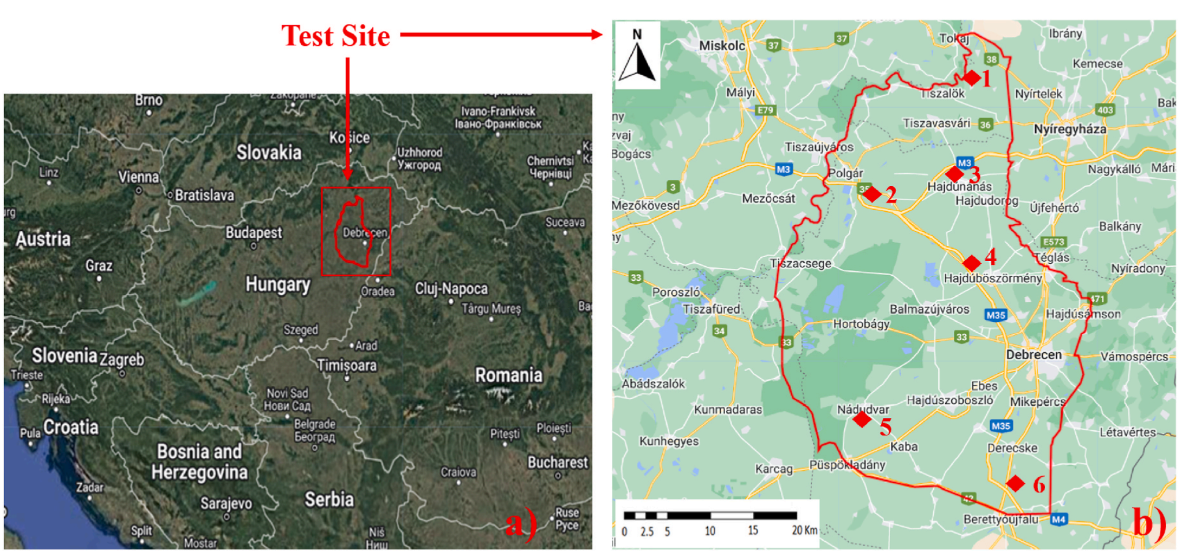

Fig. 1. (a) Regional research pilot area (test site), and (b) Meteorological stations.

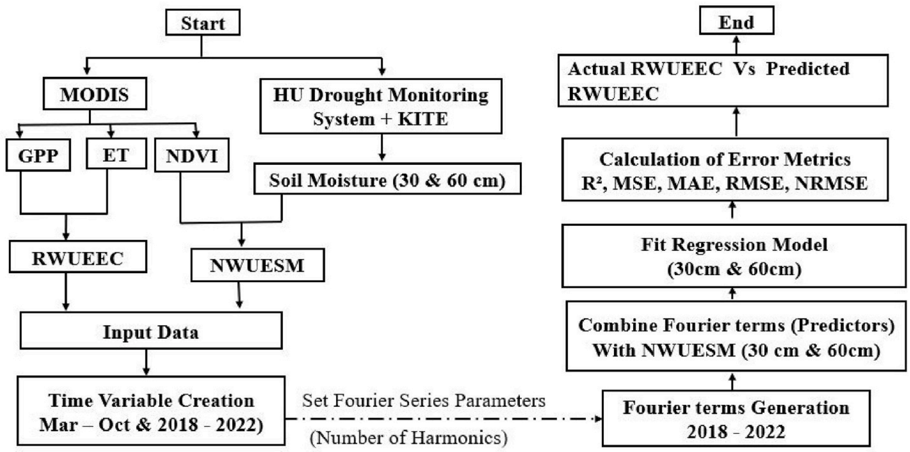

Fig. 2. Workflow showing the modeling process of WUE in the test site.

2.4.3. ET data

Evapotranspiration was obtained in google earth engine using MODIS/006/MOD16A2 dataset product, that provides global estimates of ET at an 8-day temporal and 500m spatial resolution respectively in accordance with Eq. (2). The satellite product uses the Penman-Monteith equation, incorporating key inputs such as surface meteorological data and other environmental observations to calculate potential and actual ET [44]. Other components captured in the equation include soil evaporation, canopy transpiration, and interception loss. Hence the integration of these parameters makes the MOD16A2 product deliver comprehensive ET estimates, which are particularly valuable for assessing water use and hydrological processes at regional and global scales. These estimates were in accordance with Mu et al. [45] and Monteith [44].

$$ET = \frac{\Delta(\text{R-G}) + AB\left(\frac{V}{X}\right)}{\Delta + \gamma\left(1 + \frac{Y}{X}\right)} \tag{2}$$

where ET is the actual evapotranspiration (mmday^{-1}), R is the net solar radiation (Wm^{-2}), G is the ground heat flux (Wm^{-2}), A is the air density (Kgm^{-3}), B is the specific heat of air (JKg^{-1} K^{-1}), V is the vapor pressure deficit (Pa), X is the aerodynamic resistance (sm^{-1}), Y is the surface resistance (sm^{-1}), Δ is the slope of the saturation vapor pressure curve (PaK^{-1}) and γ is the psychrometric constant (PaK^{-1}).

2.4.4. GPP data

Gross primary productivity was obtained from MODIS/006/MOD17A2H dataset product in google earth engine at an 8-day temporal and 500m spatial resolution respectively in accordance with Eq. (3). The satellite product is derived using a light-use efficiency (LUE) model, absorbed photosynthetically active radiation (PAR) and a proportion of photosynthetically active radiation (PPAR). GPP is essential for understanding carbon dynamics, productivity, and vegetation health in the assessment of the impacts of climate variability on vegetation productivity and is estimated according to Prince and Goward [46].

$$GPP = LUE \text{ x } PPAR \text{ x } PAR \tag{3}$$

Where GPP is the Gross primary productivity (gCm^{-2}day^{-1}), LUE is the light use efficiency (gCMJ^{-1}), PAR is the photosynthetically active radiation (MJm^{-2}day^{-1}), PPAR is the fraction/proportion of PAR absorbed by the vegetation.

2.5. Model development

2.5.1. Regional WUE estimation

The actual WUE for the test site was determined using the GPP and ET relationship. This was set as a benchmark for validation of our newly proposed WUE indicator following the recommendation of Lu et al. [47] who highlighted the strength of eddy covariance (EC) techniques in validating remote sensing data. The regional WUE was estimated according to Gu et al. [48] and Yang et al. [49] in accordance with Eq. (4).

$$RWUEEC = \frac{GPP}{ET} \tag{4}$$

where RWUEEC is the benchmark regional water use efficiency (gCm^{-2}mm^{-1}), GPP is the Gross primary productivity (gCm^{-2}day^{-1}), and ET is the actual evapotranspiration (mmday^{-1}).

2.5.2. Biomass soil moisture index calculation

The newly proposed biomass soil moisture indicator for calculating and predicting regional WUE was computed using input variables of NDVI and volumetric soil moisture (SM) at 30 cm and 60 cm depth respectively. The new index doesn't provide exact values of WUE but can be used in predicting WUE of a given landscape. NDVI and soil moisture ratios determined how the overall vegetation within the test site yielded per the amount of water in each soil profile depth. Although this amount of water was not directly used by the plants, it provided an indication of the amount of water available in the soil for plant uptake and monitoring soil moisture trends. We computed this relationship according to Eq. 5

$$NWUESM = \frac{NDVI}{SM} \tag{5}$$

where NWUESM is the NDVI to soil moisture relationship that is used as an indicator and predictor for regional WUE, NDVI is the Normalized Difference Vegetation Index and SM is the volumetric soil moisture content at a given soil depth.

This approach could be vital for the management of water resources as well as optimizing irrigation practices, especially in the test area that is experiencing climate variability.

2.5.3. Fourier series setup

A Fourier series regression model was set up using NWUESM at 30 cm and NWUESM at 60 cm respectively as input data to predict and capture seasonal changes of regional WUE during the cropping periods for the five consecutive years of 2018–2022 according to Eq. (17). Firstly, a dual harmonic approach comprising of a first and second harmonic were incorporated into the model to capture the seasonal vegetative growth cycles throughout the entire cropping year as well as to account for additional seasonal variations on vegetation growth attributed by environmental factors respectively [50]. The predicted regional water use efficiency (RWUEEC Pred) was computed according to Fourier [51] as a periodic function of vegetative growth with respect to the cropping months in accordance with Eq. 6

$$\text{RWUEEC Pred} = f(t) \tag{6}$$

It was necessary to model the periodic nature of vegetative growth as frequency (f) to facility the decomposition of the cropping seasonal time series. This was calculated in accordance with Eq. (7).

$$f = \frac{1}{T} \tag{7}$$

where is the frequence and t is the time in months for the vegetative growth.

Each periodic function completed a cycle of 2 π per month and 4 π for additional seasonal variations respectively within each cropping year. The annual periodicity (T_1) was computed according to Eq. (8) and seasonal variability periodicity (T_2) according to Eq. 9

$$T_1 = 2\pi. \frac{t}{12} \tag{8}$$

$$T_2 = 4\pi. \frac{t}{12} \tag{9}$$

The Fourier function f(t) with a period (T_1) was computed in accordance with Eq. (10).

$$f(t)_1 = X_\circ + \sum_{n=1}^{N}\left[X_1.sin\left(\frac{2\pi t}{12}\right) + Y_1\ cos\left(\frac{2\pi t}{12}\right)\right] \tag{10}$$

Similarly at period (T_2), we computed the Fourier function as shown by Eq. (11).

$$f(t)_2 = X_\circ + \sum_{n=2}^{N}\left[X_2.sin\left(\frac{4\pi t}{12}\right) + Y_2\ cos\left(\frac{4\pi t}{12}\right)\right] \tag{11}$$

Where N is the harmonic number considered (n = 1 and n = 2), X_1 and X_2 are the Fourier coefficients for the sine components, Y_1 and Y_2 are the Fourier coefficients for the cosine components, X_o is the average value of the periodic function across the cropping year and t for the time in months.

These coefficients were computed in accordance with Eq. (12)–(16).

$$X_o = \frac{1}{12}\int_0^{12} f(t)dt \tag{12}$$

$$X_1 = \frac{2}{12}\int_0^{12} f(t)_1 \sin\left(\frac{2\pi t}{12}\right) dt \tag{13}$$

$$Y_1 = \frac{2}{12}\int_0^{12} f(t)_1 \cos\left(\frac{2\pi t}{12}\right) dt \tag{14}$$

$$X_2 = \frac{2}{12}\int_0^{12} f(t)_2 \sin\left(\frac{4\pi t}{12}\right) dt \tag{15}$$

$$Y_2 = \frac{2}{12}\int_0^{12} f(t)_2 \cos\left(\frac{4\pi t}{12}\right) dt \tag{16}$$

The NWUESM at 30 cm and NWUESM at 60 cm values were then incorporated as external variables to predict RWUE as an output at both soil depths respectively. The prediction was in accordance with Eq. 17

$$\text{RWUEECPred} = X_o + \sum_{n=1}^{N}\left[X_1.\sin\left(\frac{2\pi t}{12}\right) + Y_1.\cos\left(\frac{2\pi t}{12}\right)\right] + \sum_{n=2}^{N}\left[X_2.\sin\left(\frac{4\pi t}{12}\right) + Y_2.\cos\left(\frac{4\pi t}{12}\right)\right] + z.\ \text{NWUESM}(30 \text{ or } 60\text{cm}) \tag{17}$$

Where z is the coefficient quantifying the influence of the variables NWUESM at 30 cm and NWUESM at 60 cm.

The Fourier series regression model in this study was chosen because of its ability to capture periodic and seasonal trends in crop growth. Its ability to handle non-linear relationships through higher-order harmonics made it ideal for time-series analysis and modeling of regional WUE across all the cropping periods [52].

2.5.4. Evaluation metrics

Error metrics were employed to quantify the similarities and deviations between the benchmark regional water use efficiency (RWUEEC) and NDVI to soil moisture-based water use efficiency predicted regional water use efficiency estimations (RWUEEC Pred). These metrics included mean squared error - MSE (Eq. (18)) that was employed to measure the error differences between observed and predicted values of water use efficiencies [53], root mean squared error - RMSE (Eq. (19)) captured the error differences between the observed and predicted values of water use efficiencies as well as the outliers present in the water use efficiency estimates [53]. The coefficient of determination – R^2 (Eq. (20)) showed the proportion of variation in the regional water use efficiency explained by the Fourier model [54], mean absolute error - MAE (Eq. (21)) showed the average magnitudes of errors between the observed and predicted values of water use efficiencies [53]. The normalized root means square error - NRMSE (Eq. (22)) captured the RMSE in percentages across the observed and predicted values of water use efficiencies [53] and lastly the Pearson's correlation coefficient (Eq. (23)) showed the strength of the linear relationship between observed and predicted values of water use efficiencies [55].

$$MSE = \frac{1}{n}\sum_{i=1}^{n}\left(P_{RWUEEC\ pred,i} - A_{RWUEEC,i}\right)^2 \tag{18}$$

$$RMSE = \sqrt{MSE} \tag{19}$$

$$R^2 = 1 - \frac{\sum_{i=1}^{n}\left(A_{RWUEEC,i} - P_{RWUEEC\ pred,i}\right)^2}{\sum_{i=1}^{n}\left(A_{RWUEEC,i} - MA_{RWUEEC}\right)^2} \tag{20}$$

$$MAE = \frac{1}{n}\sum_{i=1}^{n}\left|P_{RWUEEC\ pred,i} - A_{RWUEEC,i}\right| \tag{21}$$

$$NRMSE = \frac{RMSE}{MA_{RWUEEC}}\ x\ 100 \tag{22}$$

Where n is the total number of RWUEEC values, $P_{RWUEEC\ pred,i}$ is the ith predicted value of RWUEEC, $A_{RWUEEC,i}$ is the ith actual value of RWUEEC, and $MA_{RWUEEC,i}$ is the mean of all the Actual RWUEEC

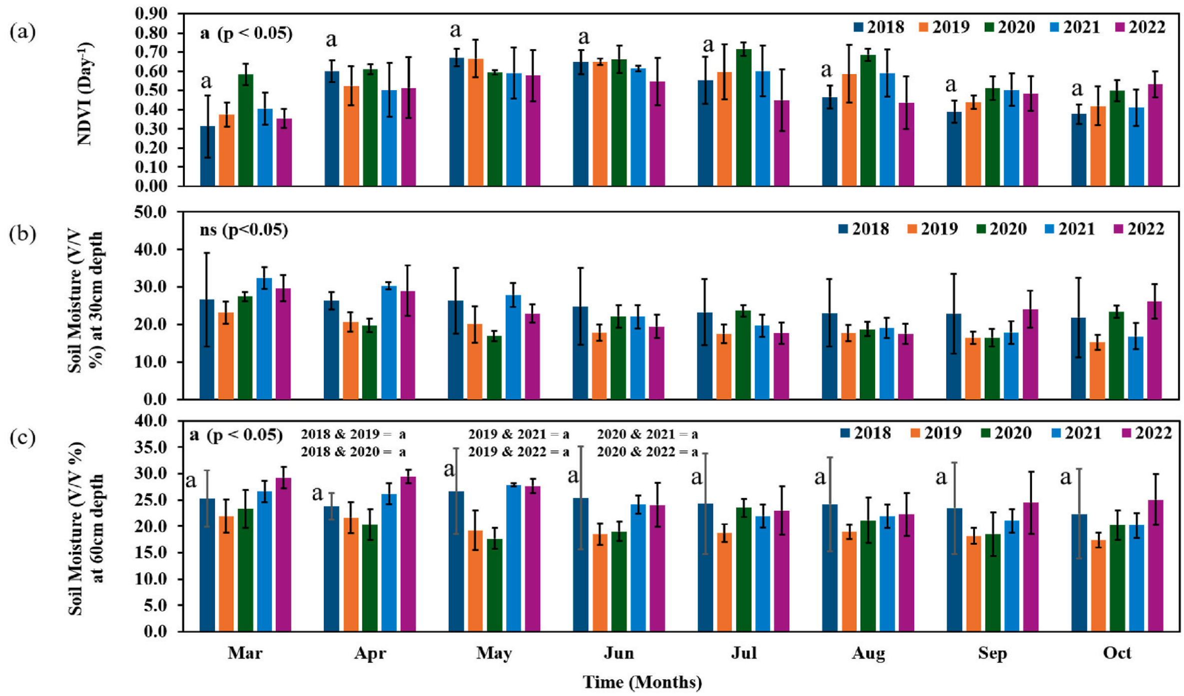

Fig. 3. Monthly mean variations of the test site; (a) NDVI, (b) Volumetric Soil moisture at 30 cm depth and (c) Volumetric Soil moisture at 60 cm root depth observed between 2018 and 2022 cropping periods. The letter (a) denotes a statistically significant difference and ns for no significant difference at $p < 0.05$.

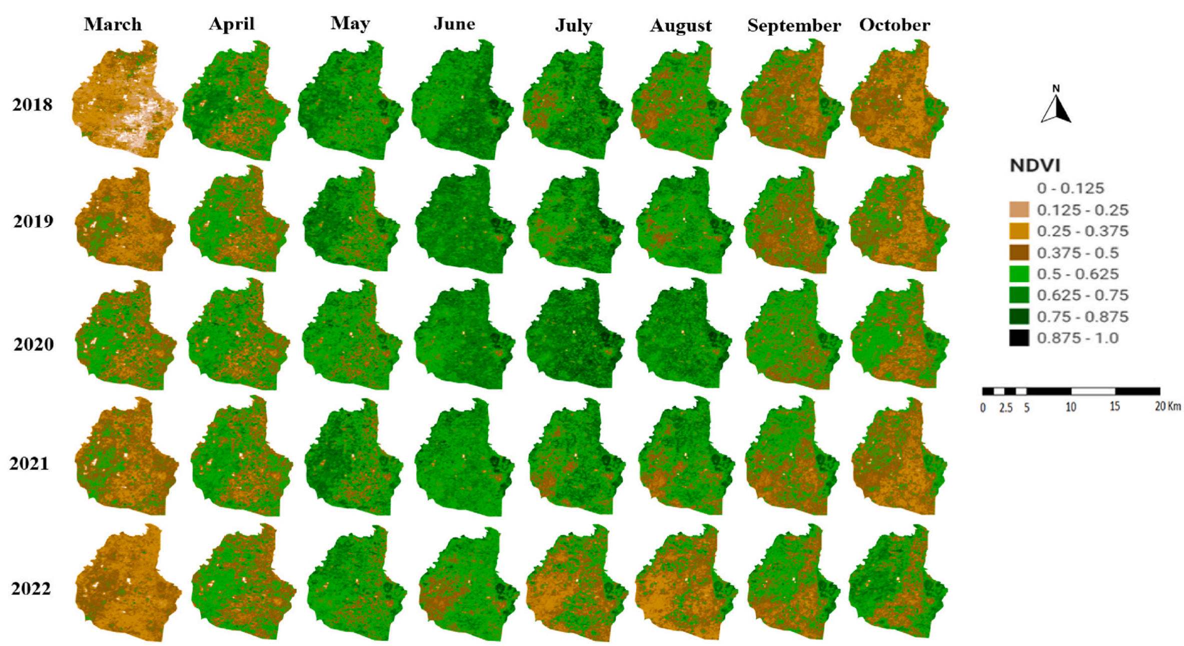

Fig. 4. NDVI time series of the test site for the cropping periods between 2018 and 2022.

2.6. Data analysis and statistics

Descriptive, statistical validation and correlation analysis were performed in MATLAB R2024b programming environment to quantify, explore and confirm the relationships within the NDVI, soil moisture, GPP and ET used in computing WUE estimates as well as the RWUEEC, NWUESM (30 cm) and NWUESM (60 cm) respectively. A pairwise comparison test using Tukey's Post Hoc analysis was also employed to the NDVI, and soil moisture between cropping months and across the five years from 2018 to 2022 respectively to identify the differences in statistical parameters.

3. Results

3.1. Spatiotemporal variation of NDVI and soil moisture content

The mean variations in the volumetric soil moisture and NDVI across the cropping periods of 2018–2022 in the test site are shown in Fig. 3a - c respectively. The months of May to July across the four consecutive cropping periods from 2018 to 2022 highlighted the peak periods of vegetation greenness (Fig. 3a), while volumetric soil moisture was highest in the months of March to May (Fig. 3b–c).

Fig. 4 shows spatial outputs of NDVI for each cropping year to compliment Fig. 3a. Relatively lower NDVI values were obtained in 2021 and 2022 respectively compared to 2018, 2019 and 2020 (Fig. 4).

The NDVI mean for 2020 (0.608) is quite higher than in 2019 (0.531), followed by 2021 (0.527), 2018 (0.502) and 2022 (0.486) respectively. Thus higher vegetation density was observed in 2020 than other years of 2019, 2021, 2018 and 2022 respectively (Fig. 4). Despite the slight differences in the NDVI values, they were not statistically significantly different across the cropping periods between 2018 and 2022 ($p = 0.1568$, $\alpha = 0.05$). However, a statistically significant difference was found between the months of 2018 ($p = 0.0000$, $\alpha = 0.05$), due to large variability in the NDVI values. The standard deviation for 2018 (0.159) is higher than that for 2019 (0.110), followed by 2020 (0.078), 2021 (0.086) and 2022 (0.072).

Considering soil moisture, the mean volumetric soil moisture content at 30 cm depth in 2018 (24.4 %) is higher than that of 2022 (23.3 %), followed by 2021 (23.27 %), 2020 (21.06 %), and 2019 (18.576 %) respectively (Fig. 3b). Similarly, the standard deviation for soil moisture at 30 cm in 2020 (6.07 %) is higher than that of 2022 (4.792 %), followed by 2020 (3.766 %), 2019 (2.538 %) and 2018 (1.842 %) respectively (Fig. 3b). No statistically significant difference was noted in the soil moisture content in the upper soil layer of 30 cm across the five cropping periods between 2018 and 2022 ($p = 0.0550$, $\alpha = 0.05$). At the deeper soil layer depth of 60 cm, the mean soil moisture content in 2022 (25.653 %) is greater than that of 2021 (24.582 %), 2020 (20.478 %), 2018 (24.424 %), and 2019 (19.305 %) respectively (Fig. 3c), indicating that soil moisture was higher in 2022 than in 2021, 2020, 2018 and 2019 respectively. The standard deviation for soil moisture at 60 cm was highest in 2021 (2.873 %) followed by 2022 (2.784 %), 2020 (2.115 %), 2019 (1.623 %) and 2018 (1.322 %) respectively (Fig. 3c). This indicates more soil moisture variability in 2021 and 2022 at 60 cm depths than 2020, 2019 and 2018 respectively. A statistically significant difference was found in the soil moisture level at 60 cm depth between the cropping periods of 2018 and 2019 ($p = 0.0005$), 2018 and 2020 ($p = 0.0095$), 2019 and 2021 ($p = 0.0029$), 2019 and 2022 ($p = 0.0000$), 2020 and 2021 ($p = 0.0447$), 2020 and 2022 ($p = 0.0004$). Also, there was a statistical significant difference across the months of 2018 ($p = 0.0000$, $\alpha = 0.05$) as shown in Fig. 3c.

The NDVI and volumetric soil moisture at 30 cm depth shows weak positive and negative correlations in March at 0.0668 and April at -0.5443 respectively (Fig. 5). During the peak crop growing stages, the correlation strengthens, reaching 0.3369 in June and peaking at 0.5727 in July and towards the end of the summer and early autumn (Fig. 5), the correlation weakens to -0.2723 in August and -0.3878 in September. By October, the correlation strengthens and becomes more positive at 0.6843 (Fig. 5). Similarly at 60 cm depth, NDVI and volumetric soil moisture content correlations are negative throughout the year with exception of October. The month of March shows a moderate negative correlation of −0.3777, and April further drops to −0.6281 (Fig. 5). During the peak vegetation growth stages, the correlation remains negative at −0.2036 in May, at −0.4987 in June, at −0.0463 in july, at −0.5739 in August and −0.2594 in September whereas in October, the correlation becomes moderately positive at 0.4548 (Fig. 5).

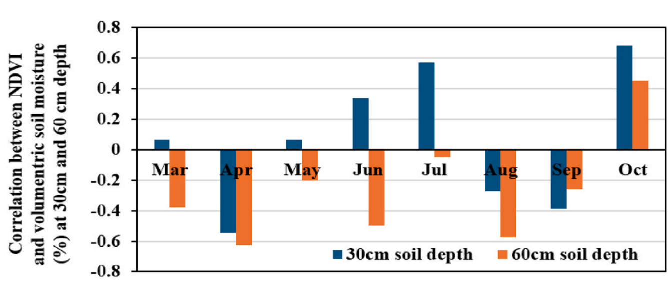

Fig. 5. Correlation between NDVI and volumetric soil moisture across the cropping months between 2018 and 2022.

3.2. Spatiotemporal variation of total rainfall, gross primary productivity and evapotranspiration

Fig. 6a shows the average monthly rainfall in millimeters across the five cropping years between 2018 and 2022 received in the test site. The month of March exhibited the lowest mean rainfall of 25.74 mm, with some notable yearly variations like 52.4 mm in 2018 and 14.1 mm in 2019. Rainfall increased in April to an average of 42.7 mm, and peaked at 64.4 mm in 2022 (Fig. 6a). The month of May showed the highest variability in the precipitation values, with a mean of 58.8 mm, a significant peak of 122.7 mm in the year 2019 and a low amount of 30.0 mm in 2022 (Fig. 6a). The month of June had the highest mean rainfall of 69.5 mm, indicated by 120.3 mm in the year 2020 with however low amounts recorded in 2021 (22.183 mm). In the month of July, rainfall remained moderately high with a mean value of 66.7 mm, and peaked at 89.027 mm in 2020 (Fig. 6a). The total rainfall then declined in August with an average of 39.04 mm, and dropping as low as 29.8 mm in 2022 (Fig. 6a). September's mean rainfall is 50.32 mm, peaking in 2022 at 99.415 mm, and the month of October experienced the lowest late-season rainfall, averaging to 35.02 mm, with extreme precipitation events totaling to 90.5 mm in 2020 and 17.9 mm in 2022 respectively (Fig. 6a). These seasonal interannual variations of rainfall greatly affects the water availability for crop production within the test region.

Fig. 6b shows GPP across the eight months from March to October between the cropping periods of 2018–2022. The highest GPP was recorded in June 2021 (66.64 $gC/m^2/day$) and April 2018 (53.43 $gC/m^2/day$). Generally, the months of March have the lowest GPP, averaging 10.86 $gC/m^2/day$ (Fig. 6b). This could be attributed to the limited vegetation activity during this month. GPP increases significantly in April, averaging 34.65 $gC/m^2/day$, due to vegetation becoming more active in terms of growth and photosynthesis. May recorded an increased average GPP of 49.89 $gC/m^2/day$, due to vigorous vegetation growth, with the highest peaks noted in 2018 (58.46 $gC/m^2/day$) and 2022 (56.57 $gC/m^2/day$). In the month of June, the highest monthly average GPP is noted at 55.71 $gC/m^2/day$, with values peaking in 2021 (Fig. 6b). The month of July also maintained strong GPP at 49.50 $gC/m^2/day$, although some values slightly decreased, with 63.16 $gC/m^2/day$ in 2020 being the highest (Fig. 6b). In the month of August, the vegetation starts to senescence and as such, GPP drops to an average value of 38.68 $gC/m^2/day$, and higher records of 51.55 $gC/m^2/day$ in 2020 (Fig. 6b). The months of September and October reflect the end of the growing season for most annual crops in the test site and thus shows low GPP, with averages of 21.82 $gC/m^2/day$ and 14.60 $gC/m^2/day$, respectively (Fig. 6b).

Furthermore, Fig 6c shows the ET values reflecting changes in vegetation activity and climatic conditions within the test site during the cropping periods of 2018–2022. The month of March had the lowest ET mean value of 9.58 mm/day, increasing gradually in April to 16.19 mm/day due to increasing temperatures and vegetation (Fig. 6c). The months of May and June recorded the highest mean ET values of 24.56 mm/day and 29.94 mm/day, respectively, which could have been attributed to peak vegetation growth and increased water demand for the crop physiological processes (Fig. 6c). Evapotranspiration started to decline in July with a mean value of 27.86 mm/day, further dropping to 20.92 mm/day in the month of August as vegetation activity slowed (Fig. 6c). The lowest ET mean values were observed in the months of September (10.62 mm/day) and October (8.23 mm/day), indicating reduced water loss at the end of the growing season due to crops reaching their physiological maturity (Fig. 6c).

3.3. Seasonal patterns of regional WUE indicators across the cropping periods of 2018–2022

Fig. 7 shows a comparison of the benchmark actual regional WUE indicator (RWUEEC) and the newly developed biomass soil moisture indicator (NWUESM). Both RWUEEC and NWUESM exhibit similar

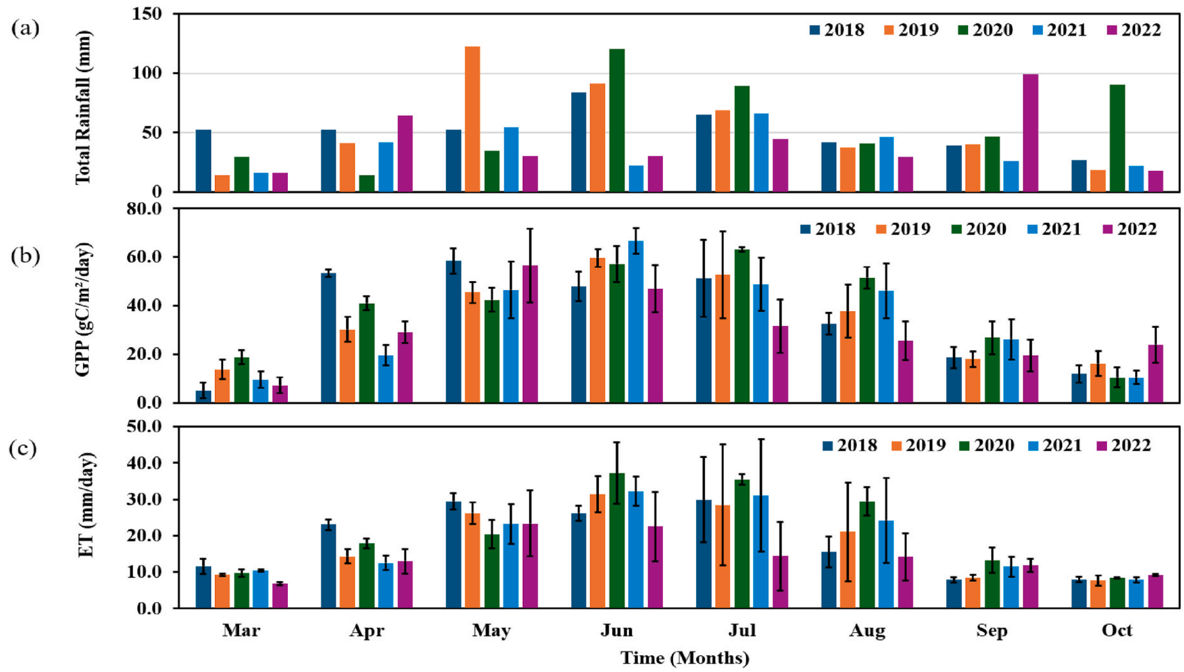

Fig. 6. Monthly variations of the Eddy Covariance variables in the TIKEVIR; (a) Total rainfall (mm), (b) Gross primary productivity (GPP) and (c) Evapotranspiration (ET) observed between 2018 and 2022 cropping Periods.

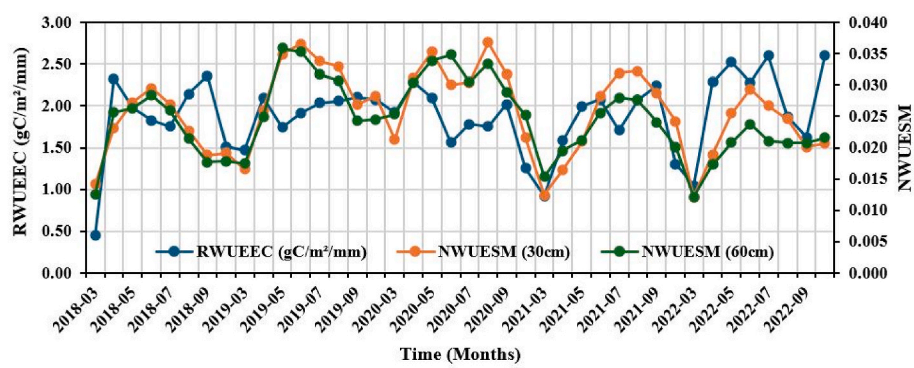

Fig. 7. Comparisons of monthly variations of regional water use efficiency estimated by a ratio of Gross primary productivity to Evapotranspiration (RWUEEC) and regional water use efficiency indicator as a ratio of NDVI to volumetric soil moisture at 30 cm and 60 cm depth respectively (NWUESM) between the cropping periods of 2018–2022.

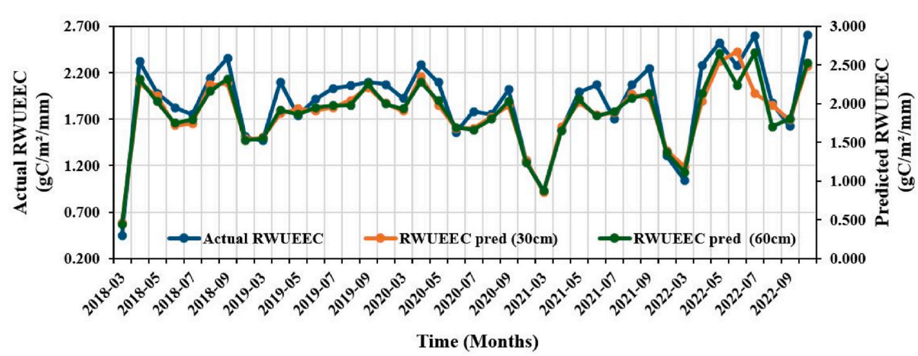

Fig. 8. Shows the seasonal pattern comparisons between the actual regional water use efficiency (RWUEEC) and predicted regional water use efficiencies (RWUEEC Pred).

seasonal trends, with relative increase and decrease in both metrics aligning over time (Fig. 7). This shows a temporal stability with higher WUE normally observed between April to September in the study site and lower WUE values observed from October to March in each cropping year. The consistent positive correlation between RWUEEC and NWUESM ensures that NWUESM at 30 cm depth reliably reflects key

Table 3
Statistical validation of the predicted regional water use efficiency (RWUEEC Pred) against the actual regional water use efficiency (RWUEEC).

RWUEEC Pred (30 cm) vs RWUEEC						RWUEEC Pred (60 cm) vs RWUEEC				
Period	R^2	MSE	RMSE	MAE	NRMSE	R^2	MSE	RMSE	MAE	NRMSE
2018	0.9817	0.006	0.0777	0.0649	4.3 %	0.9956	0.0014	0.038	0.0307	2.1 %
2019	0.6573	0.0152	0.1234	0.0997	6.4 %	0.731	0.012	0.1093	0.0988	5.7 %
2020	0.9333	0.0061	0.0782	0.0686	4.3 %	0.9486	0.0047	0.0686	0.05	3.7 %
2021	0.9042	0.017	0.1304	0.114	7.5 %	0.9158	0.015	0.1223	0.0994	7.0 %
2022	0.761	0.064	0.2529	0.2092	12.0 %	0.9452	0.0147	0.0576	0.1094	5.8 %

fluctuations in RWUEEC (Fig. 7).

Similarly, NWUESM at 60 cm shows consistent alignment with RWUEEC trends from 2018 to 2022 (Fig. 7). For example, in 2022, RWUEEC peaks in July (2.599 gC/m^2/mm), and NWUESM at 60 cm also shows a higher value of 0.021 around the same period. Between 2020-04 to 2020-10, RWUEEC drops from 2.284 gC/m^2/mm to 1.255 gC/m^2/mm, and NWUESM at 60 cm follows a similar decline from 0.030 to 0.025 (Fig. 7).

Both NWUESM at 30 cm and NWUESM at 60 cm mimic and show a synchronized seasonal pattern of RWUEEC, elaborating an effective proxy indicator for monitoring regional water use efficiency to the eddy covariance method (Fig. 7).

3.4. Correlation between RWUEEC pred and RWUEEC

Fig. 8 shows the seasonal patterns of Actual GPP-ET water use efficiency estimates (RWUEEC) against the predicted GPP-ET use efficiency obtained by inputs of NWUESM at 30 cm and NWUESM at 60 cm respectively over time (2018–2022).

The statistical validation of the relationship between the actual regional water use efficiency based on Eddy covariance parameters (RWUEEC) and the predicted regional water use efficiency (RWUEEC Pred) based on NWUESM at 30 cm and 60 cm depths between 2018 and 2022 highlighted some useful information that could be incorporated into the water management regimes in agricultural production (Table 3). The comparison of RWUEEC Pred at 30 cm and 60 cm depths respectively against RWUEEC reveals some notable distinctions in the predictive accuracies and performances of the model across the cropping periods from 2018 to 2022 (Table 3). For RWUEEC Pred at 30 cm, the coefficient of determination values (R^2) ranges from 0.6573 to 0.9817 (Table 3), indicating moderate to very strong correlations with RWUEEC. However, the performance of the model is less stable, with higher values of mean squared error (MSE), root mean squared error (RMSE) and mean squared error (MAE) in certain years. For example, 2019 had an MSE of 0.0152, RMSE of 0.1234 and 2022 an MSE of 0.064, and RMSE of 0.2529 respectively. The normalized root means square error (NRMSE) values show considerable fluctuations, particularly in 2022 with a value of 12 % (Table 3), suggesting higher variability in predicting RWUEEC at 30 cm depth. Despite some strong cropping years such as 2018 with an R^2 value of 0.9817, the overall performance is less consistent compared to RWUEEC Pred at 60 cm depth. (Table 3).

NWUESM at 60 cm exhibited a more superior and stable performance over NWUESM at 30 cm as a proxy for RWUEEC. RWUEEC Pred (60 cm) vs RWUEEC had consistently higher R^2 values above 0.7 (Table 3) and reaching as high as 0.9956 in the cropping year of 2018, demonstrating a stronger predictive power (Table 3 and Fig. 8). Furthermore, RWUEEC Pred (60 cm) has lower error metrics (MSE, RMSE, MAE, and NRMSE), across all the 5 years compared to RWUEEC Pred at 30 cm (Table 3). These statistical results suggest that NWUESM at 60 cm is a more robust and an accurate proxy for RWUEEC, with greater consistency and predictive accuracy over time (Fig. 8).

4. Discussions

4.1. NDVI and volumetric soil moisture content

The months of May to July across the five consecutive cropping periods (2018–2022) highlighted the peak periods of vegetation greenness (Fig. 3a). This could be due to the availability of optimal growth conditions such as adequate sunlight and temperatures that increased vegetation activity [30]. These environmental conditions encourage rapid growth of crops, pastures, fruit and wood trees, resulting in high NDVI values between the months of May, June and July compared to the months of March, April, August, September and October. Additionally, during these months, the test site is dominated by agricultural crops such as sunflower, corn, wheat and fodder pastures that are in their active vegetation phases contributing to high NDVI. The time series spatial analysis and monitoring of NDVI is very vital for this test site to effectively manage water resources due to its ability to provide insights into regional dynamics of the vegetation health, and general crop stand.

The cropping years of 2021 and 2022 were the dryest years due to drought effects according to the 2022 reports of the national water directorate general (OVF) and Hungarian meteorological service [30], and as such, they had the least NDVI values across the 5 consecutive cropping periods. These NDVI values are also in agreement with the total rainfall recorded in the test site between the cropping periods of March to October. For instance, the year 2020 received the highest precipitation of 465.259 mm, followed by 2019 (433.841 mm), 2018 (413.037 mm), 2022 (332.277 mm) and 2021 (294.848 mm) respectively which further justifies the impacts of water availability from rainfall and drought influences. The high variability in NDVI observed in 2018 and 2019 could indicate more diverse environmental and climatic conditions affecting biomass production. According to Gaál and Tornay [56] and the Hungarian meteorological service [30], highlighted the impacts of drought and anomalies of temperature changes. For example, they stated that between 2018 and 2020, Hungary faced drought conditions with severity persisting in 2022, affecting most parts of the country. Gaál and Tornay [56] also highlighted those annual mean temperatures of 2018 to have reached 11.93 °C and 2019 (12.86 °C) respectively against the long term annual average temperatures of Hungary (10.8 °C). The years 2020 and 2021 observed a decline in mean annual temperatures to 12.24 °C and 11.58 °C respectively and a rise to 12.62 °C in 2022. This clearly indicates climate variability faced in the test site. Therefore, Integrating NDVI results into decision-making of water resource management can develop sustainable strategies to address climate change impacts like drought, and food security.

Considering soil moisture content, the upper soil layer (30 cm) in 2018 was wetter than those of 2022, 2021, 2020 and 2019 respectively and the higher variability observed in 2020 and 2022 could have been because of drought [56]. The overall high moisture levels observed in 2021 and 2022 despite being dry years could have been attributed to supplimentation of water to support crops through irrigation.

The NDVI and volumetric soil moisture at 30 cm depth showed weak positive and negative correlations in March and April respectively

(Fig. 5), likely due to wet soils from snowmelt and minimal vegetation activity. During the peak crop growing stages between June and July, the correlation positively improves due to the vegetation heavily relying on shallow soil moisture. Towards the end of the summer and early autumn (Fig. 5), the correlation in August and September weakens due to the annual crops reaching physiological maturity and thus vegetation senescing. By October, the correlation strengthens and becomes more positive (Fig. 5) due to the role of shallow soil moisture in supporting late - season vegetation growth. Similarly at 60 cm depth, the correlation patterns are quite similar to those at 30 cm with exception of October. The month of March shows a moderate negative correlation which further drops in April (Fig. 5), which could be attributed to the minimal growth of vegetation and moisture accumulation into this depth. During the peak vegetation growth stages, the correlation remains negative in May through September due to the primary utilization of swallow depth soil moisture by the vegetation for growth. However, in October, the correlation becomes moderately positive due to the role of deeper soil moisture in supporting vegetation during the end of the season.

Similar correlations where observed in some studies conducted in humid, arid and semi-arid environments where soil moisture affected vegetation development and the vegetation in turn affected soil moisture levels in a Mutual Feedback Mechanism [57]. Higher soil moisture promoted better vegetation development, hence NDVI and soil moisture showed stronger positive correlations in the humid and sub-humid regions than in the semi-arid areas that received less precipitation [57,58]. In water-limited locations like the arid regions, negative correlations between NDVI and soil moisture content were noted due to high NDVI (vegetation growth), that reduced soil moisture through increased transpiration and root water uptake [57,58]. Additionally, they emphasized how vegetation development strained soil moisture levels during dry seasons and droughts, resulting in a feedback loop that constrained further crop growth [57]. In other similar studies, Zhao et al. [27] highlighted a positive correlation between NDVI and soil water content in the sub-humid zone to be attributed by the sub-humid zone's high precipitation, which encouraged the growth of vegetation and kept the soil moist. And due to vegetation's substantial evapotranspiration that removed water from the soil, NDVI and soil water content produced a negative correlation in the semi-arid zone [27]. According to Zhao et al. [27], dry conditions made vegetation compete for water and thus resulting in a negative correlation between NDVI and soil moisture content.

4.2. The biomass soil moisture index (NWUESM)

The prediction of actual regional WUE by NWUESM (60 cm) was stronger than the predictions of NWUESM (30 cm) because volumetric soil moisture at 60 cm depth is more stable than at 30 cm depth [59]. The deeper soil surfaces are less influenced by dynamic surface fluctuations of evaporation, rainfall impacts, and temperature changes, hence reflecting slower hydrological processes within the root zone [60]. According to G. Tang et al. [61], deeper soil depths experience minimal variability due to limited exposure to atmospheric drivers and greater buffering capacity, which results in a smoother moisture dynamic over a given time frame. The stability observed in deeper soil layers, makes deeper soil moisture at 60 cm a better indicator of the available water to crops throughout the growing season, aligning more closely with RWUEEC (Fig. 8) and Table 3. In contrast, shallow soil moisture at 30 cm fluctuates rapidly and does not accurately reflect the actual available water for transpiration, thus resulting into a weaker correlation with RWUEEC (Fig. 8) and Table 3. Some research highlights the majority of crops to rely on deeper soil water during critical growth stages when surface layers are dry [62], which further justitifes the use of deeper moisture as a stronger predictor for RWUEEC.

5. Conclusions

Throughout the growing season in the TIKEVIR region, WUE increases steadily from spring to early summer (March to June), attributed to the rising temperatures and accelerated vegetation growth that leads to efficient soil moisture usage. From the middle to late summer (July to September), WUE slightly declines after peaking in June, due to reduced soil moisture, higher temperatures, and the shift of plants from vegetative to reproductive stages. And by October (autumn), WUE decreases significantly as the growing season ends, with maturation of vegetation, and diminishing of plant activity. The WUE normally peaks around June and July corresponding to the optimal growing season for most crops and natural vegetation in the test site.

The biomass soil moisture index (NWUESM) aligns closely with the actual WUE (RWUEEC) estimated from Gross primary productivity and actual evapotranspiration across different soil depths and growing seasons, validating its reliability as a useful indicator for water use efficiency on a regional scale. NWUESM at 30 cm and NWUESM at 60 cm showed consistent positive correlation and alignment with RWUEEC trends over time with however NWUESM at 60 cm demonstrating superior accuracy and reliability compared to NWUESM at 30 cm as a proxy for RWUEEC. Our research found out that the correlation between RWUEEC Pred at 60 cm and RWUEEC showed higher R^2 values and lower error metrics (RMSE) compared to the correlation between RWUEEC Pred at 30 cm against RWUEEC, indicating the stability and precision of NWUESM at 60 cm in capturing WUE dynamics in agricultural crop production and other vegetation types in the ecosystem. This makes it a more robust and cheaper method for estimating RWUEEC across various environmental conditions. From these observations, we recommend that while irrigating crops, water should at least reach the deeper soil layers of 60 cm depth due to the stability of soil moisture, observed at this depth.

This study considers the various crop categories in the test site as a single unit of vegetation and yet different plant categories vary in their water extractions. As a result, the non-linear plant responses to soil moisture are not accounted for in the WUE estimations. Therefore, calculating regional water use efficiency as a ratio of NDVI to volumetric soil moisture is limited because NDVI reflects only the density and health of the vegetation, and not the actual biomass or water used during the entire crop physiological processes. Additionally, the volumetric soil moisture content may not accurately represent water plant availability in the heterogeneous TIKEVIR landscape. Lastly, NWUESM was only assessed at soil depths of 30 cm and 60 cm, which correspond to upper and mid-soil processes, respectively, thus the behaviour of the index in deeper soil layers was not examined and may vary for crops with deep roots. Improving the accuracy of these estimates may require measuring the water use efficiency of each crop and soil type in future studies.

CRediT authorship contribution statement

Angura Louis: Writing – original draft, Visualization, Validation, Software, Methodology, Investigation, Formal analysis, Conceptualization. **Zsolt Zoltán Fehér:** Validation, Software, Methodology, Investigation. **Tamás János:** Writing – review & editing, Resources, Funding acquisition, Data curation, Conceptualization. **Attila Nagy:** Writing – review & editing, Writing – original draft, Supervision, Resources, Methodology, Investigation, Conceptualization.

Data references

The satellite-based data sets were derived from MODIS products readily available to end users. MODIS/MCD43A4.006 NDVI: https://developers.google.com/earth-engine/datasets/catalog/MODIS_00

6_MCD43A4; MODIS/006/MOD16A2 (8-day ET): https://developers.google.com/earth-engine/datasets/catalog/MODIS_006_MOD16A2; MODIS/006/MOD17A2H (8-day GPP): https://developers.google.com/earth-engine/datasets/catalog/MODIS_006_MOD17A2H. The soil moisture data was obtained from the Hungarian drought monitoring system that also provides open access data sourcing: https://aszalymonitoring.vizugy.hu/index.php?view=info. KITE was another soil moisture data source provider who avails data upon request: https://pgr.hu/alkalmazasok.

Declaration of competing interest

The authors declare that they have no known competing financial interests or personal relationships that could have appeared to influence the work reported in this paper.

Acknowledgements

This research was carried out within the RRF 2.3.1 21 2022 00008 project, and the authors appreciate the fundings of the Széchenyi Plan Plus Program framework. We also appreciate the support given by the János Bolyai Research Scholarship of the Hungarian Academy of Sciences.

Data availability

Data will be made available on request.

References

[1] FAO, State of Food and Agriculture: Water Use and Agriculture. Reports on Global Water Scarcity and the Challenges it Poses for Agricultural Water Management Systems, FAO publications catalogue, 2023, https://doi.org/10.4060/ca7988en.
[2] FAO, The state of food and agriculture 2020. Overcoming water challenges in agriculture, Rome, https://doi.org/10.4060/cb1447en, 2020.
[3] W. Nie, B.F. Zaitchik, M. Rodell, S.V. Kumar, K.R. Arsenault, H.S. Badr, Irrigation water demand sensitivity to climate variability across the contiguous United States, Water Resour. Res. 57 (3) (2020), https://doi.org/10.1029/2020wr027738.
[4] U.N. Water, Progress on the Level of Water Stress: Global Status and Acceleration Needs for SDG Indicator 6.4.2, 2021. Food & Agriculture Organization, 2021.
[5] World Bank, Food Security Update LXVIII - August 11, 2022, 2022.
[6] C. Smith, B. Hall, F. Dentener, J. Ahn, W. Collins, C. Jones, M. Meinshausen, E. Dlugokencky, R. Keeling, P. Krummel, J. Mühle, Z. Nicholls, I. Simpson, IPCC Working Group 1 (WG1) Sixth Assessment Report (AR6) Annex III Extended data, Zenodo (CERN European Organization for Nuclear Research), https://doi.org/10.5281/zenodo.5705390, 2021.
[7] K.R. Van Daalen, C. Tonne, J.C. Semenza, J. Rocklöv, A. Markandya, N. Dasandi, S. Jankin, H. Achebak, J. Ballester, H. Bechara, T.M. Beck, M.W. Callaghan, B. M. Carvalho, J. Chambers, M.C. Pradas, O. Courtenay, S. Dasgupta, M.J. Eckelman, Z. Farooq, R. Lowe, The 2024 Europe report of the lancet countdown on health and climate change: unprecedented warming demands unprecedented action, Lancet Public Health 9 (7) (2024) e495–e522, https://doi.org/10.1016/s2468-2667(24)00055-0.
[8] A. Elbeltagi, A. Srivastava, N.L. Kushwaha, C. Juhász, J. Tamás, A. Nagy, Meteorological data fusion approach for modeling crop water productivity based on ensemble machine learning, Water 15 (1) (2022) 30, https://doi.org/10.3390/w15010030.
[9] J. Elfarkh, K. Johansen, M.M.E. Hajj, S.K. Almashharawi, M.F. McCabe, Evapotranspiration, gross primary productivity and water use efficiency over a high-density olive orchard using ground and satellite-based data, Agric. Water Manag. 287 (2023) 108423, https://doi.org/10.1016/j.agwat.2023.108423.
[10] D.L. Hoover, L.J. Abendroth, D.M. Browning, A. Saha, K. Snyder, P. Wagle, L. Witthaus, C. Baffaut, J.A. Biederman, D.D. Bosch, R. Bracho, D. Busch, P. Clark, P. Ellsworth, P.A. Fay, G. Flerchinger, S. Kearney, L. Levers, N. Saliendra, R. L. Scott, Indicators of water use efficiency across diverse agroecosystems and spatiotemporal scales, Sci. Total Environ. 864 (2022) 160992, https://doi.org/10.1016/j.scitotenv.2022.160992.
[11] G. Farquhar, M. O'Leary, J. Berry, On the relationship between carbon isotope discrimination and the intercellular carbon dioxide concentration in leaves, Funct. Plant Biol. 9 (2) (1982) 121, https://doi.org/10.1071/pp9820121.
[12] J.L. Hatfield, C. Dold, Water-use efficiency: advances and challenges in a changing climate, Front. Plant Sci. 10 (2019), https://doi.org/10.3389/fpls.2019.00103.
[13] X. Tang, H. Li, A.R. Desai, Z. Nagy, J. Luo, T.E. Kolb, A. Olioso, X. Xu, L. Yao, W. Kutsch, K. Pilegaard, B. Köstner, C. Ammann, How is water-use efficiency of terrestrial ecosystems distributed and changing on Earth? Sci. Rep. 4 (1) (2014) https://doi.org/10.1038/srep07483.
[14] J. Chang, J. Tian, Z. Zhang, X. Chen, Y. Chen, S. Chen, Z. Duan, Changes of grassland rain use efficiency and NDVI in Northwestern China from 1982 to 2013 and its response to climate change, Water 10 (11) (2018) 1689, https://doi.org/10.3390/w10111689.
[15] N. Abbasi, H. Nouri, K. Didan, A. Barreto-Muñoz, S.C. Borujeni, C. Opp, P. Nagler, P.S. Thenkabail, S. Siebert, Mapping vegetation index-derived actual evapotranspiration across croplands using the google Earth engine platform, Remote Sens. 15 (4) (2023) 1017, https://doi.org/10.3390/rs15041017.
[16] Z. Liao, B. Zhou, J. Zhu, H. Jia, X. Fei, A critical review of methods, principles and progress for estimating the gross primary productivity of terrestrial ecosystems, Front. Environ. Sci. 11 (2023), https://doi.org/10.3389/fenvs.2023.1093095.
[17] X. Luo, Y. Wang, Y. Li, Responses of ecosystem water use efficiency to drought in the Lancang–Mekong River Basin, Front. Ecol. Evol. 11 (2023), https://doi.org/10.3389/fevo.2023.1203725.
[18] J. Sheffield, E.F. Wood, M. Pan, H. Beck, G. Coccia, A. Serrat-Capdevila, K. Verbist, Satellite remote sensing for water resources management: potential for supporting sustainable development in data-poor regions, Water Resour. Res. 54 (12) (2018) 9724–9758, https://doi.org/10.1029/2017wr022437.
[19] B.S. Alharbi, Role of remote-sensing techniques in unveiling the spatiotemporal response of vegetation to climate change in the Western Makkah Province of Saudi Arabia, Environ. Chall. (2024) 100926, https://doi.org/10.1016/j.envc.2024.100926.
[20] Y. Yang, H. Guan, O. Batelaan, T.R. McVicar, D. Long, S. Piao, W. Liang, B. Liu, Z. Jin, C.T. Simmons, Contrasting responses of water use efficiency to drought across global terrestrial ecosystems, Sci. Rep. 6 (1) (2016), https://doi.org/10.1038/srep23284.
[21] A. Nagy, J. Tamás, Noninvasive water stress assessment methods in orchards, Commun. Soil Sci. Plant Anal. 44 (1–4) (2012) 366–376, https://doi.org/10.1080/00103624.2013.742308.
[22] T. Magyar, Z. Fehér, E. Buday-Bódi, J. Tamás, A. Nagy, Modelling soil moisture and water fluxes in a maize field for the optimization of irrigation, Comput. Electron. Agric. 213 (2023) 108159, https://doi.org/10.1016/j.compag.2023.108159.
[23] Y. Hu, G. Li, W. Chen, Remote sensing of ecosystem water use efficiency in different ecozones of the North China Plain, Sustainability 14 (5) (2022) 2526, https://doi.org/10.3390/su14052526.
[24] H. Wang, X. Li, J. Xiao, M. Ma, Evapotranspiration components and water use efficiency from desert to alpine ecosystems in drylands, Agric. For. Meteorol. 298–299 (2020) 108283, https://doi.org/10.1016/j.agrformet.2020.108283.
[25] E. Bwambale, F.K. Abagale, G.K. Anornu, Smart irrigation monitoring and control strategies for improving water use efficiency in precision agriculture: a review, Agric. Water Manag. 260 (2021) 107324, https://doi.org/10.1016/j.agwat.2021.107324.
[26] A. Nagy, J. Tamás, Integrated airborne and field methods to characterize soil water regime, in: A. Celkova (Ed.), Proceedings of peer-reviewed contributions, Transport of water, chemicals and energy in the soil-plant-atmosphere system], Institute of Hydrology, Slovak Academy of Sciences, Bratislava, 2009, pp. 412–420.
[27] Y. Zhao, Y. Wang, X. Zhang, L. Wang, W. Hu, T. Wang, Specific-scale correlations between soil water content and relevant climate forcing factors across two climate zones, J. Hydrol. 585 (2020) 124800, https://doi.org/10.1016/j.jhydrol.2020.124800.
[28] L. Ma, Y. Liu, X. Zhang, Y. Ye, G. Yin, B.A. Johnson, Deep learning in remote sensing applications: a meta-analysis and review, ISPRS J. Photogrammetry Remote Sens. 152 (2019) 166–177, https://doi.org/10.1016/j.isprsjprs.2019.04.015.
[29] European Commission, Integrated Tisza River Basin management plan – Update 2019, Int. Commission Protection Danube River (ICPDR) (2019) 1–125. Retrieved from, https://www.icpdr.org/sites/default/files/nodes/documents/updated_itrbmp_2019.pdf.
[30] Hungarian Meteorological Service, Climate conditions of the Tisza-Körös Valley, Retrieved from, https://www.met.hu.
[31] Hungarian Central Statistical Office, Agricultural statistics in Hungary, 2023, Retrieved from, https://www.ksh.hu, 2023.
[32] Interreg Central Europe, Pilot action middle tisza output O.T3.10 PA8, Retrieved from, https://programme2014-20.interreg-central.eu/Content.Node/TEACHER-CE/OT310-PA8-MiddleTisza-final-Copy.pdf, 2014.
[33] U.S. Department of Agriculture, Agricultural sector in Hungary faces structural changes (Report No. HU2023-0010), Retrieved from, https://apps.fas.usda.gov/newgainapi/api/Report/DownloadReportByFileName?fileName=Agricultural+Sector+in+Hungary+Faces+Structural+Changes_Budapest_Hungary_HU2023-0010.pdf, 2023, December 14.
[34] D.B. Vizi, Hydrological aspects of the low-water period of 2022 on the lowland section of the Tisza River, Műszaki Katonai Közlöny 33 (3) (2023) 103–112, https://doi.org/10.32562/mkk.2023.3.9.
[35] Hungarian Academy of Sciences, Water in Hungary, Retrieved from, https://mta.hu/data/dokumentumok/Viztudomanyi%20Program/Water_in_Hungary_2017_07_20.pdf, 2017.
[36] D.J. Vanhees, K.W. Loades, A.G. Bengough, S.J. Mooney, J.P. Lynch, Root anatomical traits contribute to deeper rooting of maize under compacted field conditions, J. Exp. Bot. 71 (14) (2020) 4243–4257, https://doi.org/10.1093/jxb/eraa165.
[37] M.N. Jaafar, L.R. Stone, D.E. Goodrum, Rooting depth and dry matter development of sunflower, Agron. J. 85 (2) (1993) 281–286, https://doi.org/10.2134/agronj1993.00021962008500020022x.
[38] Y. Zhang, J. Cao, M. Lu, P. Kardol, J. Wang, G. Fan, D. Kong, The origin of bi-dimensionality in plant root traits, Trends Ecol. Evol. 39 (1) (2023) 78–88, https://doi.org/10.1016/j.tree.2023.09.002.

[39] P. Khanal, A.J.H. Van Dijke, T. Schaffhauser, W. Li, S.J. Paulus, C. Zhan, R. Orth, Relevance of near-surface soil moisture vs. terrestrial water storage for global vegetation functioning, Biogeosciences 21 (6) (2024) 1533–1547, https://doi.org/10.5194/bg-21-1533-2024.

[40] R. He, C. Tong, J. Wang, H. Zheng, Comparison of water utilization patterns of sunflowers and maize at different fertility stages along the yellow River, Water 16 (2) (2024) 198, https://doi.org/10.3390/w16020198.

[41] G.C. Topp, J.L. Davis, A.P. Annan, Electromagnetic determination of soil water content: measurements in coaxial transmission lines, Water Resour. Res. 16 (3) (1980) 574–582, https://doi.org/10.1029/wr016i003p00574.

[42] C. Schaaf, Z. Wang, A. Strahler, MCD43A4 MODIS/Terra+Aqua BRDF/Albedo nadir BRDF-adjusted reflectance daily L3 global - 500m V006, NASA EOSDIS Land Processes DAAC (2015), https://doi.org/10.5067/MODIS/MCD43A4.006 [Data set].

[43] F.J. Kriegler, W.A. Malila, R.F. Nalepka, W. Richardson, Preprocessing transformations and their effects on multispectral recognition. Proceedings of the 6th International Symposium on Remote Sensing of Environment, 1969.

[44] J.L. Monteith, Evaporation and the Environment, vol. 19, 19th Symposia of the Society for Experimental Biology, 1965, pp. 205–234.

[45] Q. Mu, M. Zhao, S.W. Running, Improvements to a MODIS global terrestrial evapotranspiration algorithm, Rem. Sens. Environ. 115 (8) (2011) 1781–1800, https://doi.org/10.1016/j.rse.2011.02.019.

[46] S.D. Prince, S.N. Goward, Global primary production: a remote sensing approach, J. Biogeogr. 22 (4/5) (1995) 815, https://doi.org/10.2307/2845983.

[47] X. Lu, M. Chen, Y. Liu, D.G. Miralles, F. Wang, Enhanced water use efficiency in global terrestrial ecosystems under increasing aerosol loadings, Agric. For. Meteorol. 237–238 (2017) 39–49, https://doi.org/10.1016/j.agrformet.2017.02.002.

[48] C. Gu, Q. Tang, G. Zhu, J. Ma, C. Gu, K. Zhang, S. Sun, Q. Yu, S. Niu, Discrepant responses between evapotranspiration- and transpiration-based ecosystem water use efficiency to interannual precipitation fluctuations, Agric. For. Meteorol. 303 (2021) 108385, https://doi.org/10.1016/j.agrformet.2021.108385.

[49] S. Yang, J. Zhang, S. Zhang, J. Wang, Y. Bai, F. Yao, H. Guo, The potential of remote sensing-based models on global water-use efficiency estimation: an evaluation and intercomparison of an ecosystem model (BESS) and algorithm (MODIS) using site-level and upscaled eddy covariance data, Agric. For. Meteorol. 287 (2020) 107959, https://doi.org/10.1016/j.agrformet.2020.107959.

[50] H. Dette, V.B. Melas, Optimal designs for estimating individual coefficients in Fourier regression models, Ann. Stat. 31 (5) (2003), https://doi.org/10.1214/aos/1065705122.

[51] J.B.J. Fourier, Théorie analytique de la chaleur, vol. 1, Gauthier-Villars, 1888.

[52] E.O. Brigham, The Fast Fourier Transform and its Applications, Prentice Hall, 1988.

[53] C. Willmott, K. Matsuura, Advantages of the mean absolute error (MAE) over the root mean square error (RMSE) in assessing average model performance, Clim. Res. 30 (2005) 79–82, https://doi.org/10.3354/cr030079.

[54] G.H. Hardy, W.W. Rogosinski, Fourier Series, third ed., Cambridge University Press, 1962. Cambridge tracts in mathematics and mathematical physics).

[55] K. Pearson, X. Contributions to the mathematical theory of evolution. II. Skew variation in homogeneous material, Phil. Trans. Roy. Soc. Lond. 186 (1895) 343–414, https://doi.org/10.1098/rsta.1895.0010.

[56] M. Gaál, E.B. Tornay, Drought events in Hungary and farmers' attitudes towards sustainable irrigation, Idojaras 127 (2) (2023) 143–165, https://doi.org/10.28974/idojaras.2023.2.1.

[57] Z. Zhou, P. Xue, X. Zhou, T. Wang, Y. Ding, Y. Zhao, P. Chen, X. Wang, Assessing the soil moisture-vegetation mutual feedback relationship in different climatic regions of mainland China, Catena 249 (2025) 108684, https://doi.org/10.1016/j.catena.2024.108684.

[58] D. Wei, L. Yan, Z. Zhang, J. Yu, X. Luo, Y. Zhang, B. Wang, Unraveling the interplay between NDVI, soil moisture, and snowmelt: a comprehensive analysis of the Tibetan Plateau agroecosystem, Agric. Water Manag. 308 (2025) 109306, https://doi.org/10.1016/j.agwat.2025.109306.

[59] X. Hao, J. Zhang, X. Fan, H. Hao, Y. Li, Quantifying soil moisture impacts on water use efficiency in terrestrial ecosystems of China, Remote Sens. 13 (21) (2021) 4257, https://doi.org/10.3390/rs13214257.

[60] H. Liang, Y. Li, X. An, J. Liu, N. Pan, Z. Li, Soil moisture dynamics and its temporal stability under different-aged Caragana korshinskii shrubs in the loess hilly Region of China, Water 15 (13) (2023) 2334, https://doi.org/10.3390/w15132334.

[61] G. Tang, Z. Zhao, X. Jin, H. Wu, J. Li, Soil moisture content and its temporal stability in an arid aerial seeding afforestation area after 30 years vegetation restoration in China, Front. For. Glob. Change 7 (2024), https://doi.org/10.3389/ffgc.2024.1452760.

[62] P. Ramamoorthy, K. Lakshmanan, H.D. Upadhyaya, V. Vadez, R.K. Varshney, Shoot traits and their relevance in terminal drought tolerance of chickpea (Cicer arietinum L.), Field Crops Res. 197 (2016) 10–27, https://doi.org/10.1016/j.fcr.2016.07.016.